Journal of Remote Sensing & GIS
ISSN: 2469-4134

Boori et al., J Geophys Remote Sensing 2015, 4:1
DOI: 10.4172/2169-0049.1000138

Review Article Open Access

Land Surface Temperature with Land Cover Classes in ASTER and Landsat Data

Mukesh Singh Boori[1,*], **Vit Vozenílek**[1], **Heiko Balzter**[2] and **Komal Choudhary**[1]

[1]*Palacky University Olomouc, 17. listopadu 50, 771 46 Olomouc, Czech Republic*

[2]*University of Leicester, Centre for Landscape and Climate Research, UK*

[*]**Corresponding author:** Boori MS, Palacky University Olomouc, 17. listopadu 50, 771 46 Olomouc, Czech Republic, Tel: 420585634519; E-mail: mukesh.boori@upol.cz

Received date: Oct 09, 2014, **Accepted date:** Dec 22, 2014, **Published date:** Dec 29, 2014

Abstract

Land surface temperature (LST) from satellite data is a challenging task due to the atmospheric absorption and diversification of earth surface emissivity. The analysis show that land surface temperature influenced by water content or vegetation condition. The combination of HDF Explorer and ArcGIS software was useful for automatically processing the pixel latitude, longitude and brightness temperature (BT) information from the ASTER HDF and Landsat imagery files. Forest areas with more moisture and water body have shown smaller temperature than settlements. The urban area refers to the phenomenon of higher atmospheric and surface temperatures occurring in urban areas than in the surrounding vegetation areas. A lookup table of effective temperature anomalies is constructed based on the BT to resolve the inconsistencies between infrared and BT variation. Here ASTER and Landsat data show similar behavior for all land cover classes temperature. The results can be referred to similar areas of the world for LST retrieval or land surface process research, in particular under extreme bad weather conditions. So mitigation of the high temperature effects via the configuration of green spaces and sustainable designs of urban environments have become an issue of increasing concern under changing climate.

Keywords: ASTER; Landsat data; Brightness Temperature (BT)

Introduction

Brightness temperature (BT)have been used many application such as ocean salinity, soil moisture, freeze/thaw, land surface temperature, inundation function, water vapour abundance, rain fall rate, surface ocean wind speed, and vegetation structure [1,2]. LST through remote sensing is an important topic for environmental study and resource management. A number of studies and methodology carried out for LST from AMSR-E, AMSR-2, ASTER and Landsat date [3,4]. However, due to the difficulties in correcting the influences of atmospheric path and surface emissivity, the development of accurate LST algorithms is a challenging task.

Land surface information is important in emergence management during natural disasters to reduce economic loss caused by flood, droughts etc. Remote sensing of land cover classification and surface temperature has become an important research subject globally. Many methodologies use optical remote sensing data (e.g. Moderate Resolution Imaging Spectro Radiometer–MODIS) and thermal infrared satellite data to retrieve land cover classification and surface temperature. The urban area refers to the phenomenon of higher atmospheric and surface temperatures occurring in urban areas than in the surrounding vegetation areas. This phenomenon is widely observed in cities regardless of their sizes and locations [5,6]. The high temperature is mainly caused by the industrialization and urbanization [7,8]. As a result, land surface temperature (LST) increases.

The intensity of land surface temperature is based on population dynamics and development of build-up areas [9,10]. Specifically, urban structure (e.g: height-to-width ratio of buildings and streets), proportion of built-up versus green spaces per unit area, weather conditions (e.g: wind and humidity), and socioeconomic activities [11]. Land surface characteristics are primarily represented by land use/cover and the relationship between the LST and LULC has been the focus of numerous studies [12,13]. This is due to the fact that vegetation usually has higher evapotranspiration and lower emissivity than built-up areas, and thus has lower surface temperatures [14]. LST and LULC green space have negative relationship and studied by [15,16].

Study area and data

Belgrade lies 116.75 metres (383.0 ft) above sea level and is located at the confluence of the Danube and Sava rivers with coordinate of 44°49N and 20°28E. The city has an urban area of 360 square kilometres (140 sq mi), while together with its metropolitan area it covers 3,223 km^2 (1,244 sq mi). On the right bank of the Sava, central Belgrade has a hilly terrain, while the highest point of Belgrade proper is Torak hill at 303 m (994 ft). The mountains of Avala (511 m (1,677 ft)) and Kosmai (628 m (2,060 ft)) lie south of the city. Across the Sava and Danube, the land is mostly flat, consisting of alluvial plains and loessial plateaus (Figure 1).

Belgrade lies in the humid subtropical climate zone, with four seasons and uniformly spread precipitation. Monthly averages range from 1.4°C (34.5°F) in January to 23.0°C (73.4°F) in July, with an annual mean of 12.5°C (54.5°F). There are, on average, 31 days a year when the temperature is above 30°C, and 95 days when the temperature is above 25°C. Belgrade receives about 690 millimetres (27 in) of precipitation a year, with late spring being wettest. The average annual number of sunny hours is 2,112. The highest officially recorded temperature in Belgrade was +43.6°C (110 F) on 24 July 2007, while on the other end; the lowest temperature was −26.2°C (−15 F) on 10 January 1893.

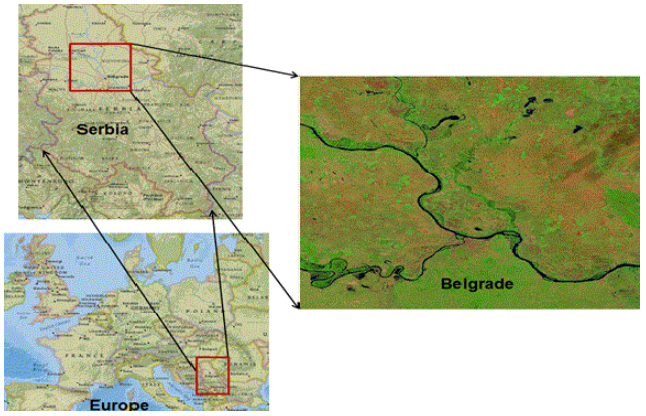

Figure 1: Study area Belgrade, Serbia.

Landsat

In this research work Landsat 8 satellite data was used. Landsat 8 carries two instruments: The operational land imager (OLI) sensor and thermal infrared sensor (TIRS). The TIRS sensor provides two thermal bands. These sensors provide improved signal-to-noise (SNR) radiometric performance quantized over a 12-bit dynamic range. This translates into 4096 potential grey levels in an image compared with only 256 grey levels in previous 8-bit instruments. Improved signal to noise performance enable better characterization of land cover state and condition. This product is delivered as 16-bit images (scaled to 55,000 grey levels). For this research work band number 11TIRS (11.5-12.51 µm) 100 m was used for surface temperature.

ASTER

ASTER data provides the user community with standard data products throughout the life of the mission. Algorithms to compute these products were created by the ASTER science team, and are implemented at the Land Processes Distributed Active Archive Centre (LP DAAC). Users can search and browse these products through GDS and NASA reverb. For this research work band number 14 TIR (10.95 - 11.65 µm) was used for surface temperature. It has 16 bit data with +/-8.55 telescope pointing capacity.

Methodology

Landsat-8 Thermal Infrared Sensor (TIRS) thermal band 11 (11. 5-12.51 µm) data with 100m resolution were utilized to derive the LST (Figure 2). The satellite data were collected on June, 2014, which was a clear day with 0% cloud cover. These variables include daily precipitation (0 mm), daily average wind speed (1.6 m/s), wind direction (South-East) and humidity (46%). Due to the lack of detailed in situ atmospheric variables that allow physical inversion of brightness temperature to LST, following algorithm was applied for retrieval of LST:

$L_\lambda = M_L Q_{cal} + A_L$

Where:

L_λ =TOAspectral radiance (w/m^{-2}/sr^{-1}/µm^{-1})
M_L=Band-specific multiplicative rescaling factor from the metadata

(RADIANCE_MULT_BAND_x, where x is the band number)
A_L=Band-specific additive rescaling factor from the metadata

(RADIANCE_ADD_BAND_x, where x is the band number)
Q_{cal}=Quantized and calibrated standard product pixel values (DN)

TIRS band data can be converted from spectral radiance to brightness temperature using the thermal constants provided in the metadata file:

$T = K_2 / (\ln (K_1 / L_\lambda + 1)$

Where:

T=At-satellite brightness temperature (K)
L_λ=TOA spectral radiance (w/m^{-2}/sr^{-1}/µm^{-1})
K_1=Band-specific thermal conversion constant from the metadata

(K_1_CONSTANT_BAND_x, where x is the band number, 10 or 11

K_2=Band-specific thermal conversion constant from the metadata

(K_2_CONSTANT_BAND_x, where x is the band number, 10 or 11)

ASTER surface temperatures are computed from spectral radiance so begins by converting DNs to radiance and for that equation is following:

L_λ=(DN - 1) X UCC

Where: L_λ is the spectral radiance, DN are the TIR band digital numbers, and UCC are the published Unit Conversion Coefficients (0.005225 w/m^{-2}/sr^{-1}/µm^{-1}).

Temperature (measured in degrees Kelvin) is then given by:

$T = K_2 / (\ln (K_1 / L_\lambda + 1)$

Where: K_1 (641.32) and K_2 (1271.22) are constants derived from Planck's radiance function.

A maximum likelihood image classification approach was applied to extract the land cover area using ArcGIS software. The four bands green, red, near-infrared, and two shortwave infrared were used for classification. It has been demonstrated that land surface temperature could be related to LCLU types [16,17]. In this study, we classified four land cover classes (forest, agriculture, settlements, and water body) to relate LST.

Results

Landsat 8 band number 11 shows 267.11 K as lowest temperature and 312.92 as highest temperatures. Maximum region show around 290 to 300 K temperatures and in ASTER, temperature range is in between 289.31 to 318.16 K (Figure 2).

To identify the behavior of each land cover class, we first selected sample sites in all four land cover classes (forest, agriculture, settlement, water body) through the use of the ArcGIS system. Then their maximum, minimum, mean, and standard deviation were derived for both Landsat and ASTER data to determine their temperature range for land cover classification. Two dimensional scatter plots between LST and land cover classes are shown in Figure 3.

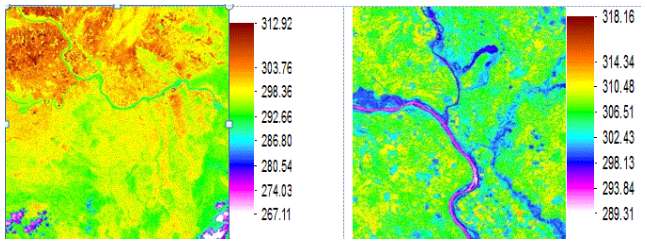

Figure 2: Landsat and ASTER data land surface temperature in study area.

There seems to be a negative linear relationship between LST and vegetation fraction or density. However, these relationships do not seem to be statistically significant enough (in all cases) to obtain meaningful conclusions. The results imply that agriculture has higher LST than forest. Settlements have highest temperature in both Landsat and ASTER data LST. Water body has lowest LST. Both data show same behavior for all land cove classes.

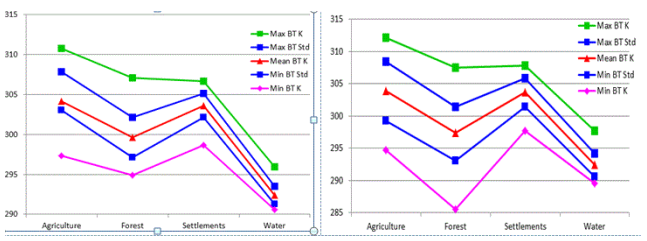

Figure 3: (a) Landsat (b) ASTER surface temperature with land cover classes.

Under changing climate, arid regions are likely to become even drier, while wet areas tend to get wetter in response to observed global warming [18] as indicated by increasing surface temperature. Expanding the green space is a rational approach for adapting to climate change. At the same time, it can contribute to the sustainable development of settlements. However, it may compete with other socio-economic interests that also require space. Therefore, in order to determine a proper balance between the sustainable development and green space increase, planners should work on it. This research will help mitigating the effects of future climate, and benefit human wellbeing by improving water and energy use efficiency.

Conclusions

This study quantitatively examined of green space on land surface temperature (LST). Normalized mutual information measure was used to quantify the relationship between LST and land cover. Our results showed that in both data green and moisture have less temperature than settlements and open area. In arid and semi-arid regions, where temperatures are already high and water resources are limited, the outcome of this study may provide climate change adaptation and mitigation benefits by reducing greenhouse gas emissions and energy demand for the cooling.

References

1. Njoku EG, Jackson T J, Lakshmi V, Chan TK, and Nghiem SV (2003) Soil moisture retrieval from AMSR-E. IEEE Transactions on Geoscience and Remote Sensing. 41:215-229.
2. Boori MS, Vozenilek V, Burian J (2014) Land-cover disturbances due to tourism in Czech Republic. Advances in Intelligent Systems and Computing, Springer International Publishing Switzerland. 303: 63-72.
3. Price JC (1984) Land surface temperature measurements from the split window channels on the NOAA 7 advanced very high resolution radiometer. J. Geosphys. Res. 89: 7231-7237.
4. Boori MS, Ferraro RR (2013) Microwave polarization and gradient ratio (MPGR) for global land surface phenology. Journal of Geology and Geosciences (JGG) 2: 1-10.
5. Connors JP, Galletti CS, Chow WTL (2013) Landscape configuration and urban heat island effects: assessing the relationship between landscape characteristics and land surface temperature in Phoenix, Arizona. Landscape Ecol. 28: 271-283.
6. Boori MS, Ferraro RR (2012) Northern Hemisphere snow variation with season and elevation using GIS and AMSR-E data. Journal of Earth Science and Climate Change (JESCC), 12: 01-06
7. Solecki WD, Rosenzweig C, Parshall L, Pope G, Clark M et al. (2005) Mitigation of the heat island effect in urban New Jersey. Global Environ. Change B: Environ. Hazards 6: 39-49.
8. Boori MS (2010) Coastal vulnerability, adaptation and risk assessment due to environmental change in Apodi-Mossoro estuary, Northeast Brazil. International Journal of Geomatics and Geosciences (IJGGS) 1: 620-638.
9. Arnfield AJ (2003) Two decades of urban climate research: A review of turbulence, exchanges of energy and water, and the urban heat island. Int. J. Climatol. 23: 1-26.
10. Boori MS, Amaro VE, Vital H (2010) Coastal ecological sensitivity and risk assessment: A case study of sea level change in Apodi River (Atlantic Ocean), Northeast Brazil. World Academy of Science, Engineering and Technology (WASET). International journal of Environmental, Earth Science and Engineering 4: 44-53.
11. Hamdi R, Schayes G (2007) Sensitivity study of the urban heat island intensity to urban characteristics. Int. J. Climatol. 28: 973-982.
12. Pu R, Gong P, Michishita R, Sasagawa T (2006) Assessment of multi-resolution and multi-sensor data for urban surface temperature retrieval. Remote Sens. Environ. 104: 211-225.
13. Boori MS, Amaro VE (2010) Detecting and understanding drivers of natural and eco-environmental vulnerability due to hydro geophysical parameters, ecosystem and land use change through multispectral satellite data sets in Apodi estuarine, Northeast Brazil. International Journal of Environmental Sciences (IJES) 1: 543-557.
14. Weng Q, Lu D, Schubring J (2004) Estimation of land surface temperature-vegetation abundance relationship for urban heat island studies. Remote Sens. Environ. 89: 467-483.
15. Chen XL, Zhao HM, Li PX, Yin ZY (2006) Remote sensing image-based analysis of the relationship between urban heat island and land use/cover changes. Remote Sens. Environ. 104: 133-146.
16. Xian G, Crane M (2006) An analysis of urban thermal characteristics and associated land cover in Tampa Bay and Las Vegas using Landsat satellite data. Remote Sens. Environ. 104:147-156.
17. Boori MS, Amaro VE (2010) Land use change detection for environmental management: using multi-temporal, satellite data in Apodi Valley of northeastern Brazil. Applied GIS International Journal 6: 1-15.
18. Durack PJ, Wijffels SE, Matear RJ (2012) Ocean salinities reveal strong global water cycle intensification during 1950 to 2000. Science 336: 455-458.